Characterizing Detection Thresholds for Six Orthogonal Modes of Vibrotactile Display Via Stylus With Precision Grasp

Ruisi Zhang, *Student Member, IEEE* and Jake J. Abbott, *Senior Member, IEEE*

***Abstract*—In this paper, we characterize the detection thresholds in six orthogonal modes of vibrotactile haptic display via stylus, including three orthogonal force directions and three orthogonal torque directions at the haptic interaction point. A psychophysical study is performed to determine detection thresholds over the frequency range 20–250 Hz, for six distinct styluses. Analysis of variance is used to test the hypothesis that force signals, as well as torque signals, applied in different directions have different detection thresholds. We find that people are less sensitive to force signals parallel to the stylus than to those orthogonal to the stylus at low frequencies, and far more sensitive to torque signals about the stylus than to those orthogonal to the stylus. Optimization techniques are used to determine four independent two-parameter models to describe the frequency-dependent thresholds for each of the orthogonal force and torque modes for a stylus that is approximately radially symmetric; six independent models are required if the stylus is not well approximated as radially symmetric. Finally, we provide a means to estimate the model parameters given stylus parameters, for a range of styluses, and to estimate the coupling between orthogonal modes.**

***Index Terms*—Pen-hold grasp, tool-mediated vibrotactile perception, magnetic haptic interface.**

I. Introduction

Vibrotactile haptic display of high-frequency vibrations enables event-based feedback [1], [2], the display of textures [3]–[6] and patterned surfaces [7]–[13], and even musical haptics [14], which can significantly enhance haptic fidelity of tool-mediated interaction with virtual or telemanipulated environments [15], [16]. Of particular interest is vibrotactile display with a pen-like stylus using a precision grasp (Fig. 1); the precision grasp is commonly used to manipulate a tool [17], and stylus-based haptic devices are commonly available commercially [18].

Although there has been significant research on characterizing humans' vibrotactile perception in terms of displacement [19]–[22], humans mainly sense acceleration during vibrotactile perception [22]–[24], which motivates studies that have considered acceleration for vibrotactile display [4], [13], [25], [26]. However, it is challenging to generate a desired vibrotactile perception in terms of acceleration since many vibrotactile displays are designed primarily to display force- and/or moment-driven vibrations in an open-loop fashion, using either the haptic device's native actuators or auxiliary actuators attached to the haptic device. There are two principal approaches to display a desired acceleration. One approach is to attach auxiliary accelerometers to close the control loop, which does not require any model, but there will be some latency in achieving the desired acceleration [4], [23], [25]. The other approach, which does not require any modification of the haptic device, is to convert desired accelerations to the corresponding torques and/or forces using an inertia model [26].

Prior works have developed dynamic models for the human hand-arm system to understand how force-driven vibrations transmit to the hand based on finite-element analysis [27], mass-spring-damper systems [28]–[33], or mechanical impedance [21], [34]. A state-of-the-art method for haptic texture display used stylus mass as a simplified inertia model to convert desired accelerations to their corresponding forces, which are then fed into the native actuators of a three-degree-of-freedom kinesthetic device [26].

Stylus-based kinesthetic haptic interfaces can render up to 6D vibrotactile stimuli—typically either 3D, 5D, or 6D—at the haptic interaction point (HIP). However, until recently, there has been little known about vibrotactile perception using torque signals (about any axis), nor how torque signals can be mapped to accelerations using inertia models. It is also unclear if the simplified inertia model used in [26] can be extended to a moment-driven vibrotactile display, since the sensation associated with a given vibration intensity is largely invariant to the direction of a force-driven vibration [20], [23], [35]–[38], but the same cannot be said for moment-driven vibrations [36]–[38]. Without an accurate inertia model—which must account for not only the inertia of the stylus (which is known), but also the effective inertia of limb (which is likely poorly understood, especially for a moment-driven vibration)—it is unclear how to display some open-loop force and/or moment to achieve a desired acceleration.

Manuscript received August 5, 2020; revised August 24, 2021; accepted August 26, 2021. Date of publication September 1, 2021; date of current version March 18, 2022. This work was supported by National Science Foundation under Grant 1423273. This article was recommended for publication by Associate Editor Hiroyuki Kajimoto and Editor-in-Chief Seungmoon Choi upon evaluation of the reviewers' comments. *(Corresponding author: Ruisi Zhang.)*

The authors are with the Department of Mechanical Engineering and the Robotics Center, University of Utah, Salt Lake City, UT 84112 USA (e-mail: ruisi.zhang@utah.edu; jake.abbott@utah.edu).

Digital Object Identifier 10.1109/TOH.2021.3109078

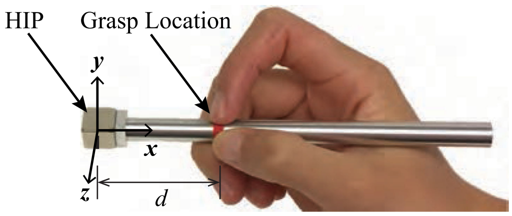

Fig. 1. Posture of a precision grasp, shown with the stylus of the magnetic haptic interface used in this study. Forces and torques are applied at the haptic interaction point (HIP). The coordinate system used defines x along the stylus, y pointing upward, and z pointing toward the subject when the stylus is held in front of the subject as shown. In general, the HIP and grasp location are separated by distance d. The stylus shown is stylus S_1 in this study.

Due to the complexity of modeling the limb-stylus inertia, in this paper, we consider vibrotactile perception in terms of the mechanical source variables (i.e., force and torque) for vibrotactile display, which directly maps the device's input variables to humans' sensations without any preconceived inertia model. Our preliminary study on which this paper is based considered each of the six orthogonal modes of stylus-based vibrotactile display and found that humans are far more sensitive to torque about the shaft of the stylus than torque orthogonal to the shaft for the frequency range of 20–250 Hz, and are less sensitive to force along the shaft than force orthogonal to the shaft at very low frequencies [36]. Our latest study proposed a weighting function that describes how the six orthogonal modes mix in the mapping to 1D vibrotactile perception [37], [38], motivated by the fact that humans cannot distinguish the direction [39] or phasing [9] of high-frequency vibrations. However, in both of these studies, we only considered a single stylus, and there is little known about how stylus parameters affect vibrotactile perceptions.

In this paper, we conduct two psychophysical experiments to determine the vibrotactile detection thresholds in each of the six orthogonal modes applied in a standard coordinate frame located at the HIP, for styluses held with a precision grasp (Fig. 1). The response variable that we use to quantify the detection threshold is the amplitude of the sinusoidal force or torque signal. We consider precision grasp holistically, without any preconceived notions about the relative sensations between the stimuli applied in the six orthogonal modes. The first experiment, which is an extension of [36], explores how the vibrotactile detection thresholds vary as a function of the frequency of the vibrotactile stimuli (i.e., the sinusoidal force or torque signals) and provides critical comparison between six orthogonal modes of vibrotactile display; this experiment considers ten frequencies within the frequency range of 20–250 Hz. The second experiment, which considers a variety of custom styluses, explores how the vibrotactile detection thresholds vary as a function of stylus parameters such as inertia, diameter at the grasp location, and the distance between the HIP and the grasp location; this experiment considers three frequencies, based on the results of the first experiment: low (20 Hz), medium (108 Hz), and high (250 Hz).

Following the two psychophysical experiments, we find minimal-parameter models, in each of the orthogonal modes, that accurately describe the vibrotactile detection thresholds across frequencies. Each model has just two free parameters that must be determined (e.g., experimentally calibrated) for a given stylus. Finally, we propose functions that can be used to estimate these free parameters for a given stylus based on the stylus parameters (i.e., without any experimental calibration). This function will be locally accurate for styluses with properties comparable to those considered in our experiments.

In our experiments, we use a magnetic haptic interface comprising an electromagnetic field source and a fully untethered stylus that has a permanent magnet attached at one end, the center of which serves as the HIP (Fig. 1). Our interface is capable of rendering vibrotactile sensations in each of the six orthogonal modes, independently, with a single stylus that can be designed as any desired shape, making it ideal for this study. Magnetic haptic interfaces differ from traditional haptic interfaces that utilize one or more back-drivable motors in a kinematic chain [1], [21], [26], [40] or one or more vibrotactile actuators attached to the stylus to render vibrations [4], [18], [33]. The dynamics of a kinematic chain may affect vibration transmission and users' vibrotactile perception. A vibrotactile actuator can only render 1D vibration, driven by either force or moment, making it challenging to render independent vibrations in different directions while controlling for actuation authority and stylus inertia properties. Although our experiments use a magnetic haptic interface, the results of our study generalize to any haptic interface using a stylus, provided the actuation applied at the HIP is a force or moment (i.e., the interface is "impedance-type").

II. Experiment 1: Effect of Frequency and Mode on Detection Thresholds

We conducted the first psychophysical experiment to generate a human-subject data set of detection thresholds for the six orthogonal modes of vibrotactile display in the frequency range of 20–250 Hz using a pen-shaped aluminum stylus. The data set was used to test the hypothesis that force signals, as well as torque signals, applied in different directions have different detection thresholds. Much of Experiment 1 was presented in [36]. Here, we went beyond [36] by adding two additional human subjects (from 10 to 12), and including a power analysis on force and torque directions for which a significant difference was not found.

A. Materials and Methods

1) Human Subjects: The psychophysical study was performed by 12 (seven male, five female) right-handed subjects, ages 23–31, who were student volunteers that gave informed consent. Subjects have normal tactile sensation and normal (corrected) vision by self-report. The study was approved by the University of Utah Institutional Review Board (IRB #00096461).

2) Apparatus: This study utilized a magnetic haptic interface (Fig. 2) that comprises two separate parts: an electromagnetic field source known as an Omnimagnet, and an untethered stylus with a cubic permanent magnet rigidly attached to one end using beeswax. The experimental

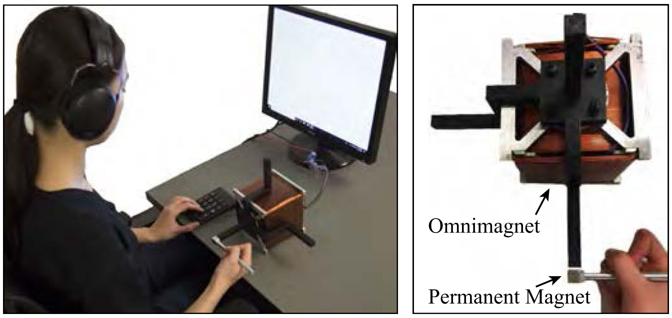

Fig. 2. (Left) Experimental setup. The magnetic haptic interface comprises an Omnimagnet electromagnetic field source and an untethered magnetic stylus. The subject holds the stylus with a precision grasp, with her forearm resting on an armrest. The monitor displays simple prompts. (Right) Close-up showing the magnetic haptic interface. The subject places the stylus's magnet at a location indicated by a given nonmagnetic rod extending from the Omnimagnet, without contacting it. Note, the configuration shown corresponds to Fig. 4(f), and the stylus shown is S_1.

apparatus enabled us to display pure forces and torques at the HIP of the stylus, which was the center of the permanent magnet, without any confounding factors related to the configuration-dependent inertia and friction found in tradition linkage-based haptic interfaces. The magnetic field from the electromagnet generates a force $\boldsymbol{f} = \nabla(\boldsymbol{m} \cdot \boldsymbol{b})$ (units N) and torque $\boldsymbol{\tau} = \boldsymbol{m} \times \boldsymbol{b}$ (units N $\cdot$ m) on the stylus's magnetic dipole $\boldsymbol{m}$ (units A $\cdot$ m^2), which can be modeled as being at the center of the cubic NdFeB permanent magnet [41]. In this experiment, we use a 12.7-mm magnet ($\|\boldsymbol{m}\| = 2.15$ A $\cdot$ m^2, 15.4-g mass). The experimental characterization of the magnetic haptic interface is described in Appendix A.

We used a radially symmetric aluminum stylus, S_1 (Figs. 1, 2, and 3), which was similar to a common pen, and which was also used in [37], [38]. A 4-mm-wide red band located at the stylus's center-of-mass indicates the desired resting position of the stylus on the subject's middle finger. The cubic permanent magnet was attached on one end; the black mark indicates the direction of the magnet's dipole moment (i.e., pointing from the south pole to the north pole), which was orthogonal to the stylus's x axis.

3) Design: We designed this experiment to enable us to investigate two distinct hypotheses. *Hypothesis 1.1:* There is a difference in detection thresholds between the three orthogonal force modes. *Hypothesis 1.2:* There is a difference in detection thresholds between the three orthogonal torque modes.

This experiment used a full-factorial repeated-measures design with two factors: the configuration of the magnetic haptic interface (Fig. 4) and the frequency of the vibration. We considered six configurations of the magnetic haptic interface (i.e., six orthogonal modes), three of which corresponded to a pure force along one of the three orthogonal axes of the stylus, and three of which corresponded to a pure torque about one of the three orthogonal axes. The ten vibration frequencies considered in this experiment were spaced evenly in a $\log_{10}$ scale within the frequency range of 20–250 Hz. This range was chosen because humans are able to detect vibrotactile stimuli in the frequency range of 20–1000 Hz [39], and most haptic interfaces cannot correctly render vibration beyond 250 Hz [1]. The above factors yielded 60 distinct combinations. The authors verified that the direction of vibration was not detectable across the entire frequency range, as expected [39].

We are interested in characterizing the vibrotactile detection threshold of the amplitude (i.e., half peak-to-peak) of the sinusoidal force or torque signal applied at the HIP, as a function of a variety of variables of interest. We used an adaptive tracking procedure (see Section II-A4) to determine the vibrotactile detection threshold of each subject for a given combination of variables. This procedure resulted in a number of reversals, which ultimately led to six best-estimate-threshold (BET) values for each combination, which were used as repeated measures in the analysis of variance (ANOVA). We performed all statistical analysis on the $\log_{10}$BET values, since humans' cutaneous systems perceive vibrotactile stimuli in this scale, based on Stevens' power law [42]. We used a mixed-effect ANOVA model to determine statistical significance in an experiment with response variable $\log_{10}$BET, with blocking factor *subject* treated as a random-effect variable, and treatment factors *mode* and *frequency* treated as fixed-effect variables. The Tukey post-hoc pairwise comparison test was run for factors found to be significant. The conventional significance for the entire analysis was determined at $\alpha = 0.05$, two tailed. Statistical analysis was performed with SPSS and MATLAB R2020a.

We performed post-hoc power analysis for the pairwise comparisons of *mode* that were found to be not significantly different. We considered each pairwise comparison to be sufficiently powered if it would be capable of detecting a difference equal to the just noticeable difference (JND) in amplitude discrimination if such a difference existed (using the conventional power of $1 - \beta = 0.8$, two tailed). The difference $\Delta\mu$ that could have been detected is

$$\Delta\mu = t^* \sqrt{\frac{S_1^2}{n_1} + \frac{S_2^2}{n_2}}, \tag{1}$$

where S_j is the standard deviation in $\log_{10}$BET of data set j, n_j is the sample size for data set j, and t^* is the critical value. The Bonferroni correction suggested using a significance of $\alpha^* = \alpha/10 = 0.005$ for each of the ten individual pairwise comparisons (i.e., ten frequencies), which corresponds to a critical value of 2.8. Combined with a critical value of 0.84 for the desired power of 0.8, we considered a total critical value of $t^* = 2.8 + 0.84 = 3.64$. Prior studies reported the JND in amplitude discrimination of 0.4–6 dB (for various quantities) in the frequency range of 20–250 Hz, which reached its highest value (i.e., 6 dB) when the intensity of the vibrotactile stimulus is close to the detection threshold [22], [43]–[47]. Thus, we concluded that there was sufficient power for any individual pairwise comparison (i.e., between two particular modes at a given frequency) when the difference $\Delta\mu$ calculated using (1) was not greater than $\log_{10}2$ (i.e., 6 dB converted to a $\log_{10}$ scale).

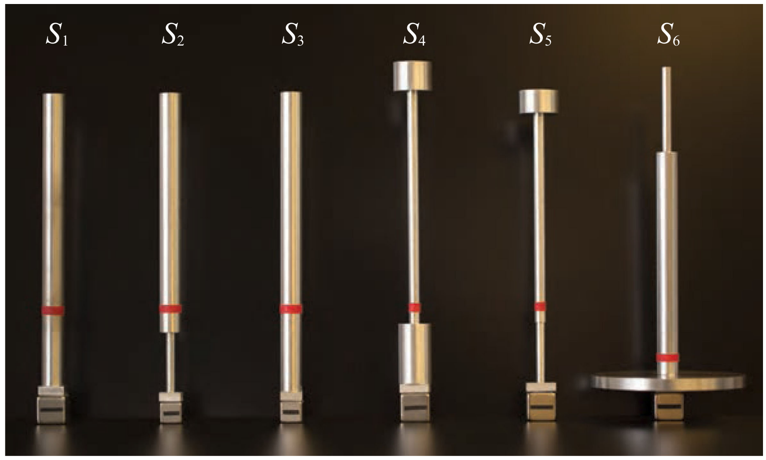

(a) Six styluses fabricated for this study.

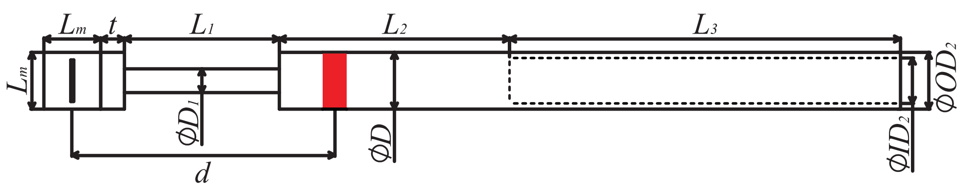

(b) Definition of stylus parameters.

	S_1	S_2	S_3	S_4	S_5	S_6
m (g)	41.2	20.7	26.0	41.2	28.8	84.9
I_{xx} (g·mm^2)	719	283	352	1.05×10^3	731	2.83×10^4
$I_\perp$ (g·mm^2)	8.67×10^4	3.54×10^4	4.33×10^4	1.28×10^5	9.30×10^4	8.67×10^4
d (mm)	44.1	44.7	44.5	44.1	43.6	22.0
D (mm)	9.53	9.53	9.53	4.76	4.76	9.53
t (mm)	4.00	4.00	4.00	4.00	4.00	2.03
L_1 (mm)	-	26.0	-	26.2	26.2	5.08
D_1 (mm)	-	4.00	-	14.4	3.81	67.3
L_2 (mm)	127	38.6	68.4	101	90.9	96.5
L_m (mm)	12.7	9.53	9.53	12.7	12.7	12.7
L_3 (mm)	-	65.6	61.8	12.7	10.2	37.1
ID_2 (mm)	-	7.62	7.01	-	-	-
OD_2 (mm)	-	9.53	9.53	16.9	17.4	4.06

(c) Stylus parameters. In S_2–S_6, the parameters highlighted gray are held approximately constant with respect to the corresponding parameters of S_1, and the parameters highlighted pink are varied by a factor of approximately 2 relative to those of S_1. The direction of x, y, and z are consistent with Fig. 1. I_{xx} and $I_\perp$ are obtained about the center-of-mass of the stylus, not the HIP. $I_\perp = I_{yy} = I_{zz}$ indicates the rotational inertia about both axes that are orthogonal to the axis of stylus.

Fig. 3. Styluses used in this study. Each stylus comprises (at most) three cylindrical sections, with a cuboid section on which a cubic permanent magnet is attached. The center-of-mass of the complete stylus is indicated by the red band.

4) Procedure: Experiment 1 was conducted in six sessions, each considering a single mode and lasting 35–50 minutes per subject. For a given subject, the sessions were separated by at least 48 hours to mitigate the effect of the configuration order [48]. The order of the sessions was randomized for each subject.

At the beginning of a session, the subject sat in front of the table with the apparatus on it (Fig. 2). A 100-mm-long non-magnetic rod attached to a given side of the Omnimagnet indicated the desired position of the stylus. The subject was instructed to rest their forearm on the armrest, hold the stylus using a precision grasp with the center of the middle finger contacting the red band, and place the center of the stylus's permanent magnet very close to the end of the given rod without contacting it. Before the experiment began, the subject was allowed to adjust the height of the chair, the height of the armrest, and the position of the Omnimagnet on the table to facilitate a comfortable posture while holding the stylus in a precision grasp. Subjects were instructed to use a grasp force consistent with how they would comfortably hold a pen for

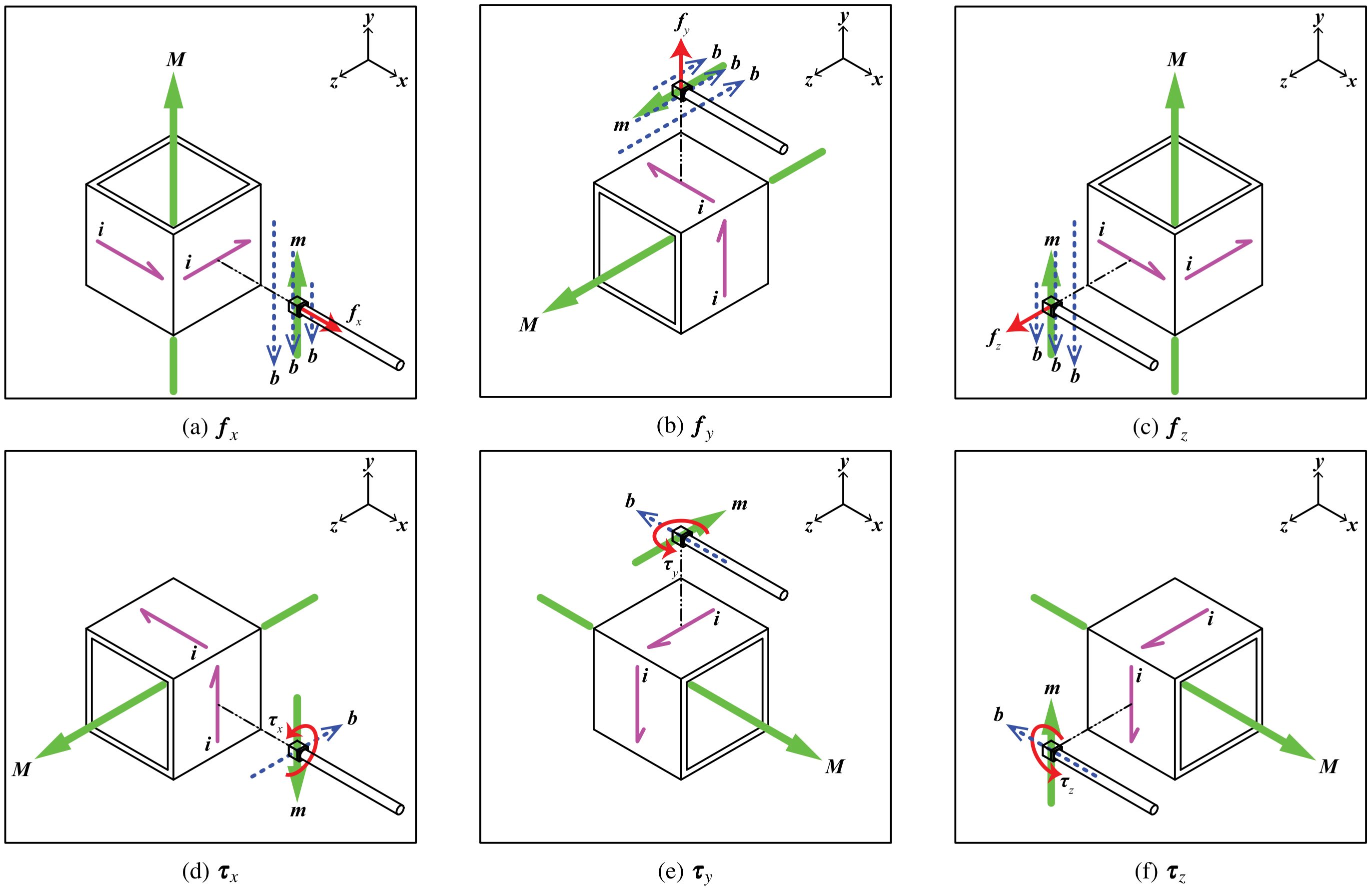

Fig. 4. The six configurations of the magnetic haptic interface used in this study, which each excite one of the six orthogonal modes. When current i flows through the electromagnet as shown, it generates the corresponding dipole moment M located at the electromagnet's center. The permanent magnet's dipole moment $\boldsymbol{m}$ is located at its center. The top three configurations correspond to a force mode along a given orthogonal axis, due to the spatial derivative of the field: $\boldsymbol{f} = \nabla(\boldsymbol{m} \cdot \boldsymbol{b})$. The bottom three configurations correspond to a torque mode about a given orthogonal axis, as the stylus's dipole attempts to align with the field: $\boldsymbol{\tau} = \boldsymbol{m} \times \boldsymbol{b}$. When the current is varied sinusoidally in time, the magnitude of the resulting force or torque varies sinusoidally in time as well.

writing. We note that all six configurations (Fig. 4) enabled the subject to hold the stylus in the same orientation. The subject wore ear muffs for the duration of the experiment to eliminate audio cues from the device and other distractions. A 508 mm (20 in) monitor, placed at an approximate distance of 700 mm from the subject, provided a visual display.

In a given session, the order of the ten frequencies was randomized for each subject. The subject was given no information about the vibration parameters. The procedure to determine the BET for a given frequency was as follows. A two-interval forced-choice (2-IFC) psychophysical design [49] and a one-up, two-down adaptive tracking procedure [50] was used to determine the BET of the subject for a given frequency. A single 2-IFC trial included two samples: one sample that did not vibrate the stylus, and one that did, presented in a random order. Each sample lasted 1.5 s with a number "1" or "2" simultaneously displayed on the monitor. Each 2-IFC trial forced the subject to choose which sample had the vibration (whether or not they could perceive one). There was a pause after each trial to allow the subject to indicate, either verbally or with a show of fingers, which sample had the vibration; the response was manually recorded by the experimenter, after which she began the next trial. The one-up, two-down adaptive tracking procedure determined the amplitude of the vibration signal for each trial. This procedure was started at a high amplitude that is easily felt (determined during pilot testing among the authors), decreased after two successive correct responses, then increased after any single incorrect response, and finally stopped at the 15th reversal. The amplitude was multiplied/divided by 2 for an increase/decrease, respectively, in the first three reversals, and then by $\sqrt{2}$ in the remaining 12 reversals. The final 12 reversal amplitudes were used to estimate the threshold for a given frequency, which in turn is the threshold for a given combination. Each reversal amplitude corresponding to a change from increasing to decreasing was paired with the next reversal amplitude corresponding to a change from decreasing to increasing. The BET for each pair was computed as the geometric mean of the two reversal amplitudes [51]. Each frequency (i.e., combination) resulted in six BETs (from the final 12 reversals), which were used as repeated measures in the ANOVA.

After half of the session was complete (i.e., after five frequencies were complete), the subject was forced to take a break of at least 5 minutes to eliminate fatigue. The subject could also take a break at any time during the session if requested.

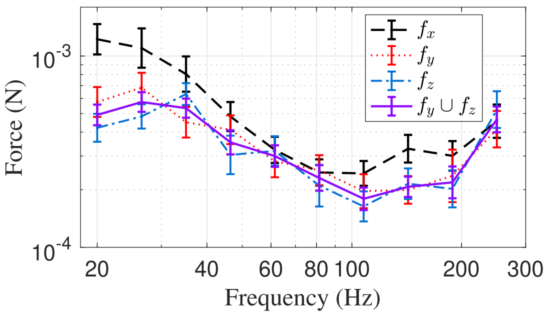

Fig. 5. BET (means with 95% CI) for the orthogonal force modes, for all frequencies and subjects tested, where $f_y \cup f_z$ is the union of the f_y and f_z data sets.

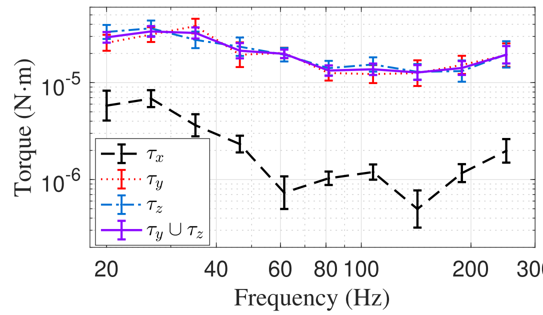

Fig. 6. BET (means with 95% CI) for orthogonal torque modes, for all frequencies and subjects tested, where $\tau_y \cup \tau_z$ is the union of the τ_y and τ_z data sets.

B. Results

1) Comparison of Force Modes (Hypothesis 1.1): Figure 5 shows the experimental results for BET, for all frequencies tested, for the three pure-force configurations (Figs. 4(a), 4(b), and 4(c)). For each of the three orthogonal force modes (i.e., the three pure-force configurations), there was a clear trend of BET being relatively high (i.e., the subjects are relatively insensitive) at the lowest frequencies, with the BET decreasing with increasing frequency to a minimum value (i.e., frequencies at which the subjects are most sensitive), and then BET increasing with further increases in frequency. After verifying the normality and sphericity assumptions are met, a within-subjects two-way ANOVA with *mode*, *frequency*, and their interaction for all three orthogonal force modes (i.e., 30 combinations) showed the effect of *mode* was statistically significant ($F = 11.3$, $p < 0.01$), as was the effect of *frequency* ($F = 17.9$, $p < 0.001$), but the effect of their interaction was not significant. A Tukey post-hoc pairwise comparison test for *mode* showed the difference between f_x and f_y and the difference between f_x and f_z were statistically significant ($p < 0.001$ in each case), but the difference between f_y and f_z was not significant.

A post-hoc pairwise power test between f_y and f_z for all frequencies tested indicated that the desired power of 0.8 was reached for all frequencies except 189 Hz. Considering the substantial overlap of the confidence intervals at 189 Hz, we felt comfortable reaching the conclusion that f_y and f_z were largely equivalent across frequencies. This enabled us to establish a new data set $f_y \cup f_z$, which is the union of the f_y and f_z data sets, in order to increase the power of the statistical tests to follow.

Using the two data sets f_x and $f_y \cup f_z$, after verifying the normality and sphericity assumptions are met, a within-subjects two-way ANOVA with *mode*, *frequency*, and their interaction for both orthogonal force modes (i.e., 20 combinations) showed the effect of *mode* was statistically significant ($F = 38.1$, $p < 0.001$), as was the effect of *frequency* ($F = 19.0$, $p < 0.001$), but the effect of their interaction was not significant. A Tukey post-hoc pairwise comparison test between f_x and $f_y \cup f_z$ for all frequency tested showed the differences at 20–35 Hz and at 142 Hz were statistically significant ($p < 0.005$ in each case), but the differences at all other six frequencies were not significant. For each of these six frequencies, a post-hoc pairwise power test between f_x and $f_y \cup f_z$ indicated that the desired power of 0.8 was reached. For each of the four frequencies found to have significant differences, $\log_{10}$BET due to f_x was higher than due to $f_y \cup f_z$, meaning subjects were less sensitive to force signals along the shaft of the stylus than to the two force signals orthogonal to the shaft (which were the same as each other) at these frequencies.

2) Comparison of Torque Modes (Hypothesis 1.2): Figure 6 shows the experimental results for BET, for all frequencies tested, for the three pure-torque configurations (Figs. 4(d), 4(e), and 4(f)). As with forces, for each of the three orthogonal torque modes (i.e., three pure-torque configurations), there was a clear trend of BET being relatively high (i.e., the subjects were relatively insensitive) at the lowest frequencies, with the BET decreasing with increasing frequency to a minimum value (i.e., frequencies at which the subjects were most sensitive), and then BET increasing with further increases in frequency. After verifying the normality and sphericity assumptions are met, a within-subjects two-way ANOVA with *mode*, *frequency*, and their interaction for all three orthogonal torque modes (i.e., 30 combinations) showed the effect of *mode* was statistically significant ($F = 176.0$, $p < 0.001$), as was the effect of *frequency* ($F = 17.4$, $p < 0.001$), but the effect of their interaction was not significant. A Tukey post-hoc pairwise comparison test for *mode* showed the difference between τ_x and τ_y and the difference between τ_x and τ_z were statistically significant ($p < 0.001$ in each case), but the difference between τ_y and τ_z was not significant.

A post-hoc pairwise power test between τ_y and τ_z for all frequencies tested indicated that the desired power of 0.8 was reached for all frequencies except 250 Hz. Considering the substantial overlap of the confidence intervals at 250 Hz, we felt comfortable reaching the conclusion that τ_y and τ_z were largely equivalent across frequencies. This enabled us to establish a new data set $\tau_y \cup \tau_z$, which is the union of the τ_y and τ_z data sets.

Using the two data sets τ_x and $\tau_y \cup \tau_z$, after verifying the normality and sphericity assumptions are met, a within-subjects two-way ANOVA with *mode*, *frequency*, and their interaction for both orthogonal torque modes (i.e., 20 combinations) showed the effect of *mode* was statistically significant ($F = 287.2$, $p < 0.001$), as was the effect of *frequency* ($F = 17.4$, $p < 0.001$), but the effect of their interaction was not significant. A Tukey post-hoc pairwise comparison test for *frequency* and *mode* showed that, at all frequencies, the differences between τ_x and $\tau_y \cup \tau_z$ was statistically significant ($p < 0.005$ in each case). BET due to τ_x was significantly lower than due to $\tau_y \cup \tau_z$ at all frequencies, with a large effect size; the BET means of τ_x were approximately three times lower than the BET means due to $\tau_y \cup \tau_z$ at the lowest frequencies, and were approximately 25 times lower at the frequencies of peak sensitivity. This means that subjects were substantially more sensitive to torque signals about the shaft of the stylus than torque signals about the two axes orthogonal to the shaft (which were the same as each other).

III. Experiment 2: Effect of Stylus Parameters on Detection Thresholds

The results of Experiment 1 are for a specific stylus. We conducted the second psychophysical experiment to generate a human-subject data set of detection thresholds for the six orthogonal modes of vibrotactile display, for a variety of custom styluses, for three frequencies (based on the results of the Experiment 1): low (20 Hz), medium (108 Hz), and high (250 Hz). The data set was used to test the hypothesis that detection thresholds are affected by a number of stylus parameters: inertia, diameter at the grasp location, and the distance between the HIP and the grasp location.

A. Methods

1) Human Subjects: The same human subjects that participated in Experiment 1 participated in Experiment 2.

2) Apparatus: This experiment utilized the same magnetic haptic interface described in Experiment 1. We used five aluminum styluses, S_2–S_6 (Fig. 3). Using S_1 from Experiment 1 as the reference stylus, we designed the five new styluses to each reduce one parameter by a factor of 2—including the mass (S_2), moment of inertia about three axes (S_3), the diameter of the cylindrical section at the grasp point (S_4 and S_5), and the distance between the center of the permanent magnet (i.e., the HIP) and the stylus's center-of-mass (S_6)—while holding other relevant parameters constant. We assume that the other uncontrolled parameters will not affect the vibrotactile perception in a given mode, due to the expected dynamics of the vibration mode. In this experiment, we used two different permanent magnets: a 9.53-mm magnet ($\|\boldsymbol{m}\| = 1.02$ A $\cdot$ m^2, 6.48-g mass) for styluses S_2 and S_3; and a 12.7-mm magnet ($\|\boldsymbol{m}\| = 2.15$ A $\cdot$ m^2, 15.4-g mass) for styluses S_4, S_5, and S_6.

3) Design: We designed this experiment to enable us to investigate ten distinct hypotheses, as enumerated in Table I. Each hypothesis considers if a certain stylus parameter affects the detection threshold in a certain direction, and that test involves a comparison between two styluses. For example, Hypothesis 2.1 considers if stylus mass m affects the detection threshold for f_x, and it involves a comparison between styluses S_1 and S_2.

TABLE I
The Ten Hypotheses of Experiment 2 and Their Results

Hypotheses			Results		
#	Hypothesis	Styluses	F	p	Correlation
2.1	m affects f_x	S_1, S_2	23.3	0.001	positive
2.2	D affects f_x	S_1, S_4	5.5	0.04	positive
2.3	$I_\perp$ affects $f_y \cup f_z$	S_1, S_3	15.4	0.002	positive
2.4	D affects $f_y \cup f_z$	S_1, S_5	34.0	<0.001	positive
2.5	d affects $f_y \cup f_z$	S_1, S_6	62.6	0.006	negative
2.6	I_{xx} affects τ_x	S_1, S_3	7.4	0.02	positive
2.7	D affects τ_x	S_1, S_5	0.01	0.9	
2.8	$I_\perp$ affects $\tau_y \cup \tau_z$	S_1, S_3	22.6	0.001	positive
2.9	D affects $\tau_y \cup \tau_z$	S_1, S_5	54.2	<0.001	positive
2.10	d affects $\tau_y \cup \tau_z$	S_1, S_6	2.2	0.2	

Experiment 2 uses a fractional-factorial repeated-measures design with three treatment factors: the *mode* (Fig. 4), the *frequency* of vibration, and the *stylus* (Fig. 3). We consider the same six configurations as in Experiment 1, but at only three vibration frequencies (20 Hz, 108 Hz, and 250 Hz), which are a subset of the ten frequencies considered in Experiment 1. The results from Experiment 1 showed a similar trend of BET for all six modes within the frequency range 20–250 Hz for S_1. The three frequencies that were chosen to capture the overall trend: 20 Hz and 250 Hz are the lowest and highest frequencies within the frequency range tested, with moderate sensitivity, and the BET at approximately 108 Hz reaches the minimum value, where subjects are most sensitive. We implicitly assume that a change of stylus parameters will not substantially affect this overall trend. The three stylus parameters considered in this experiment are the stylus inertia, the stylus diameter at the grasp location, and the distance between the HIP and the grasp location. The distance between the HIP and the grasp location is considered for the four modes f_y, f_z, τ_y, and τ_z; the other parameters are considered for all six modes. We only consider the stylus inertia in the direction of the corresponding vibration mode and assume the unconsidered inertias do not affect the vibrotactile sensations in that mode. The mass corresponds to f_x, the moment of inertia about the axis of the stylus corresponds to τ_x, and the moment of inertia orthogonal to the axis of the stylus corresponds to f_y, f_z, τ_y, and τ_z. We tested the following stylus-mode combinations: S_2 and S_4 with f_x; S_3 and S_5 with all modes excluding f_x; and S_6 with all modes excluding f_x and τ_x. This yields 48 distinct parameter sets.

We use a mixed-effect ANOVA model to determine statistical significance in an experiment with response variable $\log_{10}$BET, with blocking factor *subject* treated as a random-effect variable, and treatment factors treated as fixed-effect variables, which are *frequency* for all *Hypotheses 2.1–2.10*, *inertia* for *Hypotheses 2.1, 2.3, 2.6*, and *2.8*, *diameter* for *Hypotheses 2.2, 2.4, 2.7*, and *2.9*, and *distance* for *Hypotheses 2.5* and *2.10*.

We performed post-hoc power analysis for the pairwise comparisons of styluses that were found to be not significantly different. We consider each pairwise comparison to be sufficiently powered if it would be capable of detecting a difference $\Delta\mu$ from (1) equal to the just noticeable difference (JND) in amplitude discrimination if such a difference existed (using the conventional power of $1 - \beta = 0.8$, two tailed). The Bonferroni correction suggests to use a significance of $\alpha^* = \alpha/3 = 0.017$ for each of the three individual pairwise comparisons (i.e., three frequencies), which corresponds to a critical value of 2.4. Combined with a critical value of 0.84 for the desired power of 0.8, we consider a total critical value of $t^* = 2.4 + 0.84 = 3.24$. Similar to the post-hoc power test for *Experiment 1*, we conclude there is sufficient power for any individual pairwise comparison (i.e., between two particular modes at a given frequency) when the difference $\Delta\mu$ calculated using (1) is not greater than $\log_{10}2$ (i.e., 6 dB converted to a $\log_{10}$ scale).

4) Procedure: Experiment 2 was conducted in 6 sessions, with each session considering a single mode (i.e., configuration) and lasting 35–50 minutes per subject. Most of the procedure was the same as previously described for Experiment 1. However, we made the following changes for Experiment 2. The subject was required to change stylus once or twice within the session, with the order of the styluses, and subsequently the frequencies, in a given session randomized. The subject was forced to take a break of at least 1 minute when the experimenter changed the stylus (i.e., after three frequencies are complete). Finally, the subject manually input their response using a numeric keypad.

B. Results

After verifying the normality and sphericity assumptions were met, a within-subjects two-way ANOVA with *frequency*, the specific stylus parameter of interest, and their interaction for each hypothesis was performed. For all ten hypotheses, the main effect of *frequency* was statistically significant (as expected from Experiment 1). The results for the main effect of the specific stylus parameter of interest are provided in Table I; we include the F statistic and p value. For each parameter in which a significant effect was found, we indicate if there was a positive or negative correlation between a change in the stylus parameter of interest and the respective detection threshold. For all ten hypotheses, the interaction between *frequency* and the stylus parameter was not statistically significant.

There were two hypotheses for which a statistically significant effect of the stylus parameter on the respective detection threshold was not found. For Hypothesis 2.7, a post-hoc pairwise power test between S_1 and S_5 for all three frequencies tested indicates that the desired power of 0.8 was reached for all frequencies tested except 20 Hz. For Hypothesis 2.10, a post-hoc pairwise power test between S_1 and S_6 for all three frequency tested indicates that the desired power of 0.8 was reached for all frequencies tested.

IV. Parametric Modeling of Detection Thresholds

In this section, we utilize the results of Experiment 1 to first develop a parametric model that characterizes the role of frequency on detection thresholds in each of the six principal modes. Then, using the results of Experiment 2, we expand the model to incorporate the role of stylus parameters and identify model parameters that are invariant to stylus parameters.

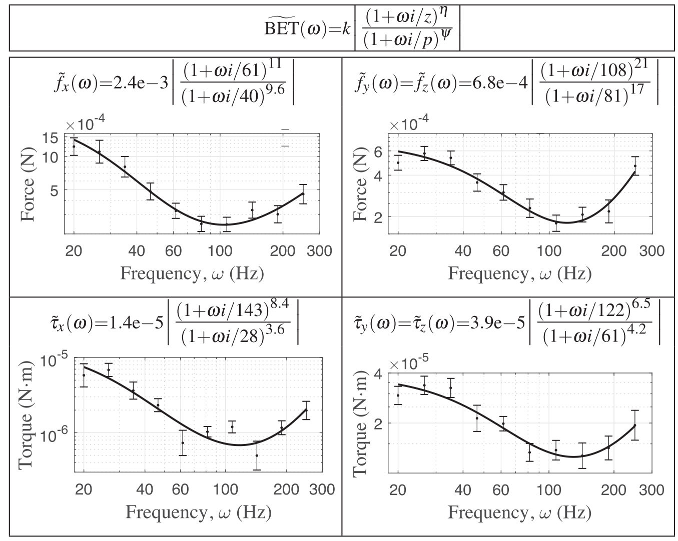

Fig. 7. Measured BET values for stylus S_1 (mean with 95% confidence intervals in $\log_{10}$ scale) and estimated BET values using four independent five-parameter models.

A. Characterizing the Role of Frequency

We propose a simple yet effective model that characterizes the detection thresholds (units N for the force modes and units $\mathrm{N} \cdot \mathrm{m}$ for the torque modes) as a function of the frequency ω (units Hz) of the sinusoidal vibrotactile stimulus displayed at the HIP. After observing the shape of the curves in Figs. 5 and 6 from Experiment 1, and inspired by frequency-response plots of transfer functions (i.e., Bode magnitude plots), we hypothesized that we could fit a five-parameter model of the form

$$\widetilde{\mathrm{BET}}(\omega) = k\left|\frac{(1+\omega i/z)^{\eta}}{(1+\omega i/p)^{\psi}}\right| \tag{2}$$

to each of the principal modes, where i is the imaginary unit.

The performance of such a model, for mode j, can be evaluated using the mean square error

$$\mathrm{MSE}_j = \frac{1}{N}\sum_{n=1}^{N}\Big(\log_{10}(\widetilde{\mathrm{BET}}_j(\omega_n)) - \log_{10}(\mathrm{BET}_j(\omega_n))\Big)^2 \tag{3}$$

where $\log_{10}\mathrm{BET}_j(\omega_n)$ is the mean value across all subjects, and $\widetilde{\mathrm{BET}}_j(\omega_n)$ is the model's predicted threshold, for each of the $N = 10$ frequencies tested. We consider the threshold values in a $\log_{10}$ scale because humans' cutaneous sensing perceives vibrotactile stimuli in this scale [42].

Using our complete data set for stylus S_1, we use gradient-descent to minimize MSE for each of the four models

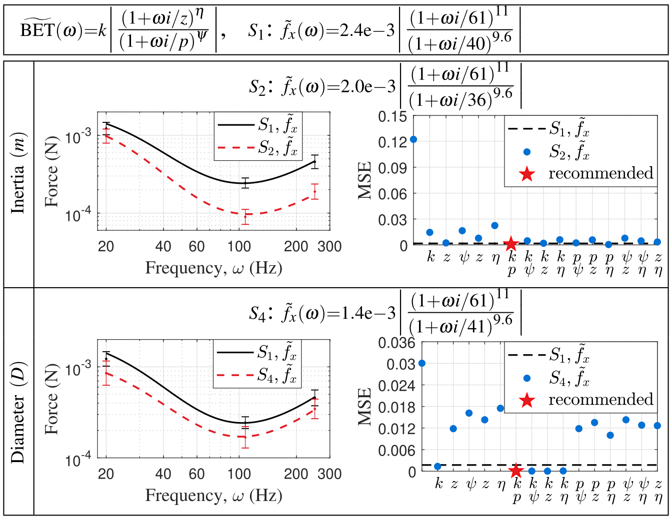

Fig. 8. (Left) Measured BET $f_x(\omega)$ values for styluses S_1, S_2, and S_4 (mean with 95% confidence intervals in $\log_{10}$ scale), and estimated BET values using the recommended two-parameter model. (Right) MSE for styluses S_2 and S_4 in which only one or two parameters are varied from the baseline model for S_1.

independently. Fig. 7 shows the four resulting five-parameter models. We see that the models do a good job of capturing the detection thresholds across frequencies.

B. Incorporating the Role of Stylus Parameters

Next, we determine the role of stylus parameters in the five-parameter models, using the data set of Experiment 2. We simultaneously identify parameters in those models that are invariant to stylus parameters and can thus be considered constant. The result is minimal-parameter models for each of the principal modes.

Let us begin with our model for the f_x mode, which will enable us to describe our methodology that we will apply to all of the independent modes. From Experiment 2, we know that both the inertia m (i.e., S_2 vs. S_1) and diameter D (i.e., S_4 vs. S_1) affect the detection thresholds in the f_x mode, but what is not clear is which of the five parameters in the model of S_1 must be changed in order to account for changes in these parameters. Beginning with the model for S_1, we allow each of the five parameters to vary one at a time, and then two at a time, and fit new minimum-MSE models (now with $N = 3$) to the f_x mode for each of S_2 and S_4. As shown in Fig. 8, a model with just two free parameters is sufficient to describe the f_x mode across stylus parameters:

$$\tilde{f}_x(\omega) = k_{f_x}\left|\frac{(1+\omega i/61)^{11}}{(1+\omega i/p_{f_x})^{9.6}}\right| \tag{4}$$

The other three parameters in the original five-parameter model can be treated as constants that are invariant to stylus parameters. We can now repeat this process for the other modes.

We know that the inertia $I_{yy} = I_{zz}$ (i.e., S_3 vs. S_1), the diameter D (i.e., S_5 vs. S_1), and the distance d (i.e., S_6 vs. S_1)

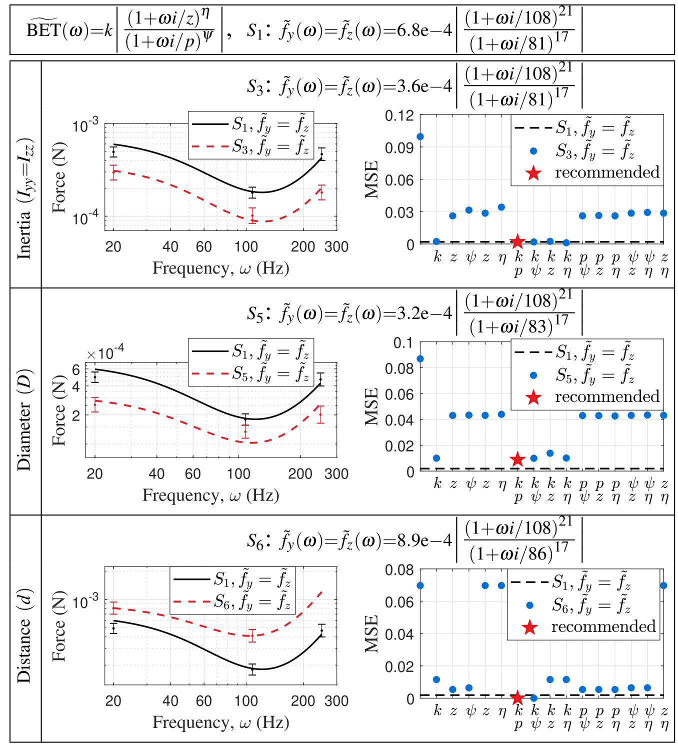

Fig. 9. (Left) Measured BET $f_y(\omega) = f_z(\omega)$ values for styluses S_1, S_3, S_5, and S_6 (mean with 95% confidence intervals in $\log_{10}$ scale), and estimated BET values using the recommended two-parameter model. (Right) MSE for styluses S_3, S_5, and S_6 in which only one or two parameters are varied from the baseline model for S_1. Note: Measured BET is not presented at 250 Hz for S_6 because four subjects could not detect even the highest-magnitude force signals (7.70 mN) that our experimental system can render at 250 Hz.

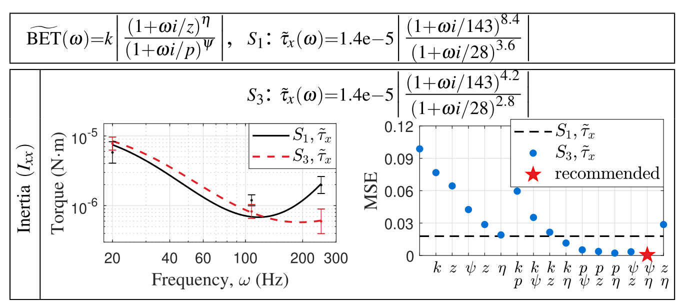

Fig. 10. (Left) Measured BET $\tau_x(\omega)$ values for styluses S_1 and S_3 (mean with 95% confidence intervals in $\log_{10}$ scale), and estimated BET values using the recommended two-parameter model. (Right) MSE for stylus S_3 in which only one or two parameters are varied from the baseline model for S_1.

affect the detection thresholds in the f_y and f_z modes. As shown in Fig. 9, a model with just two free parameters is sufficient to describe the f_y and f_z modes across stylus parameters:

$$\tilde{f}_y(\omega) = \tilde{f}_z(\omega) = k_{f_{y,z}}\left|\frac{(1+\omega i/108)^{21}}{(1+\omega i/p_{f_{y,z}})^{17}}\right| \tag{5}$$

We know that the inertia I_{xx} (i.e., S_3 vs. S_1) and the diameter D (i.e., S_5 vs. S_1) affect the detection thresholds in the τ_x mode. As shown in Fig. 10, a model with just two free parameters is sufficient to describe the τ_x mode across stylus parameters:

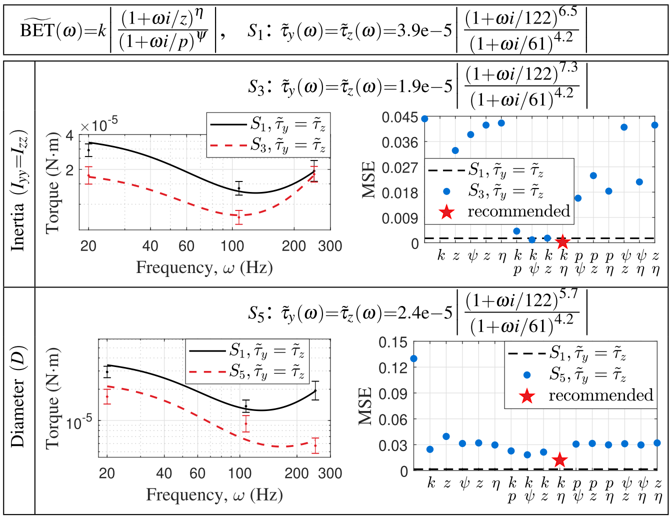

Fig. 11. (Left) Measured BET $\tau_y(\omega) = \tau_z(\omega)$ values for styluses S_1, S_3, and S_5 (mean with 95% confidence intervals in $\log_{10}$ scale), and estimated BET values using the recommended two-parameter model. (Right) MSE for styluses S_3 and S_5 in which only one or two parameters are varied from the baseline model for S_1.

$$\tilde{\tau}_x(\omega) = 1.4\text{e}{-5}\left|\frac{(\omega i/143)^{\eta_{\tau_x}}}{(\omega i/28)^{\psi_{\tau_x}}}\right| \tag{6}$$

Finally, we know that the inertia $I_{yy} = I_{zz}$ (i.e., S_3 vs. S_1), the diameter D (i.e., S_5 vs. S_1), and the distance d (i.e., S_6 vs. S_1) affect the detection thresholds in the τ_y and τ_z modes. As shown in Fig. 11, a model with just two free parameters is sufficient to describe the τ_y and τ_z modes across stylus parameters:

$$\tilde{\tau}_y(\omega) = \tilde{\tau}_z(\omega) = k_{\tau_{y,z}}\left|\frac{(1+\omega i/122)^{\eta_{\tau_{y,z}}}}{(1+\omega i/61)^{4.2}}\right| \tag{7}$$

V. Discussion

Using the results of this study, it is possible to utilize the geometric and inertial properties of the stylus of a haptic display to estimate how a given high-frequency sinusoidal force or torque rendered at the HIP compares to the threshold that will be detected. If this result is combined with the maximum force and torque values that can be commanded at the HIP of a given haptic display, one can determine the most efficient way to deliver vibrotactile sensations, potentially considering actuation authority that is already being used for the kinesthetic display.

It is important to remember that the results of this study are most applicable to stylus's that have geometric and inertial properties similar to that of S_1. Our local sensitivity analysis only considered changes in those properties by a factor of two. For a new stylus that differs from S_1 more substantially, the models developed here may lose accuracy, so extrapolation should be done with caution.

The result that $\tilde{f}_y = \tilde{f}_z$ and $\tilde{\tau}_y = \tilde{\tau}_z$ should be assumed to be contingent upon the stylus in question being accurately approximated as radially symmetric. If that were not the case, we would expect that separate model parameters would be required for each of these four modes. As a result, we would expect a total of 12 independent parameters, rather than eight, to be required.

Below, we discuss some of the ways in which our results might be extended for practical application with a given haptic display.

A. Estimating Model Parameters From Stylus Parameters Using Linear Interpolation

The four models derived in Section IV-B have a total of eight independent parameters to characterize a given stylus. For a new stylus, these parameters could be fit experimentally. Here, we provide an alternative method to estimate the parameter values by linearly interpolating the models that were fit to the six styluses of this study. We provide equations that can be used to estimate each of the model parameters, as well as the range of the stylus parameters for which the model is an interpolation of experimental values. We note that we have not shown that the model parameters are linear with respect to the stylus parameters, so this method should be viewed as an approximation. Further, additional care should be taken when applying these equations for stylus parameters that are outside of the range provided.

The model parameters k_{f_x} and p_{f_x} can be estimated over the range of stylus parameters $m \in [20.7, 41.2]$ g and $D \in [4.76, 9.53]$ mm as

$$k_{f_x} = (2.015\text{e}{-5})m + (2.110\text{e}{-4})D - 4.617\text{e}{-4} \tag{8}$$
$$p_{f_x} = (1.567\text{e}{-1})m - (2.041\text{e}{-1})D + 35.14 \tag{9}$$

The model parameters $k_{f_{y,z}}$ and $p_{f_{y,z}}$ can be estimated over the range of stylus parameters $I_\perp = I_{yy} = I_{zz} \in [8.67\text{e}4, 9.30\text{e}4]$ g $\cdot$ mm^2, $D \in [4.76, 9.53]$ mm, and $d \in [22.0, 44.5]$ mm as

$$k_{f_{y,z}} = (7.457\text{e}{-9})I_\perp + (8.772\text{e}{-5})D - (9.239\text{e}{-6})d - 3.901\text{e}{-4} \tag{10}$$

$$p_{f_{y,z}} = (9.466\text{e}{-6})I_\perp - (2.802\text{e}{-1})D - (1.962\text{e}{-1})d + 91.86 \tag{11}$$

The model parameters ψ_{τ_x} and η_{τ_x} can be estimated over the range of stylus parameters $I_{xx} \in [352, 719]$ g $\cdot$ mm^2 as

$$\psi_{\tau_x} = (2.166\text{e}{-3})I_{xx} + 2.037 \tag{12}$$
$$\eta_{\tau_x} = (1.147\text{e}{-2})I_{xx} + 1.995\text{e}{-1} \tag{13}$$

Finally, the model parameters $k_{\tau_{y,z}}$ and $\eta_{\tau_{y,z}}$ can be estimated over the range of stylus parameters $I_\perp = I_{yy} = I_{zz} \in [4.33\text{e}4, 9.30\text{e}4]$ g $\cdot$ mm^2 and $D \in [4.76, 9.53]$ mm as

$$k_{\tau_{y,z}} = (4.471\text{e}{-10})I_\perp + (3.593\text{e}{-6})D - 3.421\text{e}{-5} \tag{14}$$
$$\eta_{\tau_{y,z}} = -(1.739\text{e}{-5})I_\perp + (1.378\text{e}{-1})D + 6.699 \tag{15}$$

B. Dimensional Reduction

In this study, we characterized six orthogonal 1D vibrotactile stimuli independently, each as a function of frequency and stylus parameters. In our prior study [37], which only considered a single stylus (S_1) and a single frequency (108 Hz) as noted earlier, we considered a full 6D vibrotactile stimulus and found that a quadratic weighting function of the form

$$\tilde{P} = V^\top W V \tag{16}$$

can be used to predict the 1D normalized stimulus (i.e., the detection threshold is indicated by $\tilde{P} = 1$), where $V = [f_x\ f_y\ f_z\ \tau_x\ \tau_y\ \tau_z]^\top$ is the signed magnitudes of the six principal modes at a common frequency, and W is a positive-semi-definite weighting matrix whose elements serve a dual purpose of normalizing the stimulus values and describing the coupling between the six orthogonal modes. It is our conjecture in [37] that a simple fitting procedure may be possible with only knowledge of the diagonal elements of W: experimentally determine the diagonal elements, then set $W_{23} = W_{32} = \sqrt{W_{22}W_{33}}$ and $W_{45} = W_{54} = 0.1\sqrt{W_{44}W_{55}}$ to maintain the coupling relationships.

We can now combine our current and prior results. We can view the weighting matrix W for a given stylus as a function of frequency:

$$W = \begin{bmatrix} \frac{1}{\tilde{f}_x(\omega)^2} & 0 & 0 & 0 & 0 & 0 \\ 0 & \frac{1}{\tilde{f}_y(\omega)^2} & \frac{1}{\tilde{f}_y(\omega)\tilde{f}_z(\omega)} & 0 & 0 & 0 \\ 0 & \frac{1}{\tilde{f}_y(\omega)\tilde{f}_z(\omega)} & \frac{1}{\tilde{f}_z(\omega)^2} & 0 & 0 & 0 \\ 0 & 0 & 0 & \frac{1}{\tilde{\tau}_x(\omega)^2} & \frac{0.1}{\tilde{\tau}_x(\omega)\tilde{\tau}_y(\omega)} & 0 \\ 0 & 0 & 0 & \frac{0.1}{\tilde{\tau}_x(\omega)\tilde{\tau}_y(\omega)} & \frac{1}{\tilde{\tau}_y(\omega)^2} & 0 \\ 0 & 0 & 0 & 0 & 0 & \frac{1}{\tilde{\tau}_z(\omega)^2} \end{bmatrix}. \tag{17}$$

where the values in W can be found using (4)–(7). This makes the assumption that the coupling relationships observed for stylus S_1 at 108 Hz will hold for different styluses and frequencies. We note that (17) assumes neither $\tilde{f}_y = \tilde{f}_z$ nor $\tilde{\tau}_y = \tilde{\tau}_z$, such that it will generalize to a stylus that cannot be accurately approximated as being radially symmetric. It is also interesting to note that τ_x and τ_y are coupled in their perception, whereas we have shown herein that it is $\tilde{\tau}_y$ and $\tilde{\tau}_z$ that can described by the same functions (assuming a radially symmetric stylus). Using the above formulation, we can predict the 1D normalized vibrotactile stimulus for a given 6D vibrotactile stimulus in the frequency range of 20–250 Hz, assuming the stylus under consideration has properties that are comparable to those of the six styluses considered here.

If the new stylus is substantially different from S_1, and it was determined that (17) was not properly capturing the coupling relationship, a new weighting matrix could be found using the methodology of [37], [38].

VI. Conclusion

In this paper, we characterized the detection thresholds in the six principal modes of vibrotactile haptic display via stylus, including three orthogonal force directions and three orthogonal torque directions at the haptic interaction point. A psychophysical study was performed to determine detection thresholds over the frequency range 20–250 Hz, for six distinct styluses. Analysis of variance was used to test the hypothesis that force signals, as well as torque signals, applied in different directions have different detection thresholds. We found that people are less sensitive to force signals parallel to the stylus than to those orthogonal to the stylus at low frequencies, and far more sensitive to torque signals about the stylus than to those orthogonal to the stylus. Optimization techniques were used to determine four independent two-parameter models to describe the frequency-dependent thresholds for each of the principal force and torque modes for a stylus that is approximately radially symmetric. Six independent models are required if the stylus is not well approximated as radially symmetric. Finally, we provided a means to estimate the model parameters given stylus parameters, for a range of styluses, and to estimate the coupling between orthogonal modes.

Appendix A
Characterization of the Haptic Interface

The magnetic haptic interface (Fig. 2) used in this study comprises an Omnimagnet (i.e., electromagnetic field source) and an untethered stylus with a permanent magnet attached, which is used to display pure forces and torques at the HIP of the stylus.

An Omnimagnet [52] comprises three mutually orthogonal nested coils with a spherical ferromagnetic core in the center, with a design that was optimized to maximize the accuracy of the dipole field model as a description of its field:

$$\boldsymbol{b}(\boldsymbol{p}) = \frac{\mu_0}{4\pi\|\boldsymbol{p}\|^5}\left(3\boldsymbol{p}\boldsymbol{p}^T - \|\boldsymbol{p}\|^2 I\right)\boldsymbol{M} \tag{18}$$

where $\boldsymbol{M}$ (units A $\cdot$ m^2) is the dipole moment of the Omnimagnet, $\boldsymbol{p}$ (units m) is a vector measured from the center of the Omnimagnet to a point of interest, $\mu_0 = 4\pi \times 10^{-7}$ T $\cdot$ m$\cdot$A^{-1} is the permeability of free space, I is the identity matrix, and $\boldsymbol{b}$ (units T) is the resulting magnetic field vector at the point of interest. To avoid confounding factors, in this study we utilize only the middle coil of the Omnimagnet. Its dipole strength is proportional to its current i (units A) as $\|\boldsymbol{M}\| = 6.87i$ A$\cdot$ m^2.

We characterized the frequency response of the coil using a dynamic signal analyzer (Hewlett Packard 35665 A), as shown in Fig. 12. The gain data set can be interpolated for any frequency in the range of interest. This enables us to compensate for high-frequency attenuation, and generally have an understanding of what currents (and thus, what magnetic fields) are being generated at any given frequency given some sinusoidal voltage input. We are not concerned with phase lag, since it cannot be perceived [9].

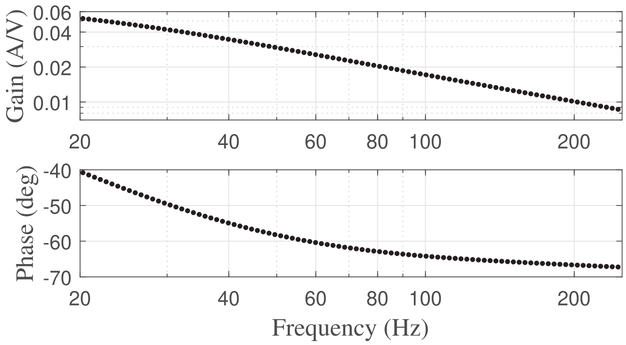

Fig. 12. Frequency-response plot of output current due to input voltage, for the middle coil of the Omnimagnet. The magnitude (i.e., half peak-to-peak) of the input sinusoidal voltage signal used to generate the data is 1.10 V.

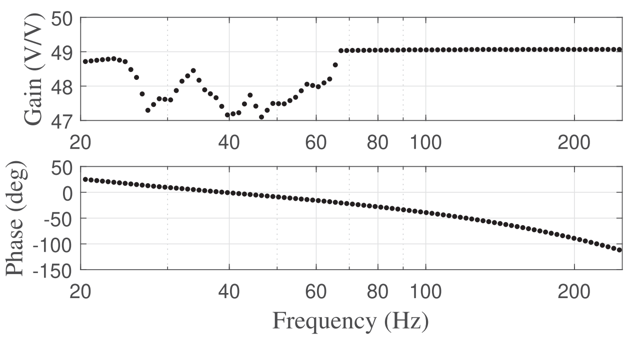

Fig. 13. Frequency-response plot of output voltage due to input voltage, for the audio amplifier connected to the middle coil of the Omnimagnet. The magnitude (i.e., half peak-to-peak) of the input sinusoidal voltage signal used to generate the data is 1.10 V.

The electromagnet is powered by a class D audio amplifier (Crown XLS 2002), capable of 1050 W of maximum output power for frequencies of 20 Hz to 20 kHz. The frequency response of the amplifier connected to (i.e., loaded by) the coil was measured by the dynamic signal analyzer in the 20–250 Hz frequency range; the results are shown in Fig. 13. The amplifier's gain can be approximated as constant at 48.5 with less than 2.9% error across the frequencies of interest. The amplifier's phase plot appears to show a combination of a 1.3 ms delay and a high-pass-filter behavior; however, we are not concerned with the phase lag, since it cannot be perceived [9].

The amplifier is given an audio signal from a PC running a MATLAB program that creates sinusoidal voltage signals, which are generated by a onboard sound card (Realtek ALC 887). These sinusoidal signals are fed into the amplifier, which outputs a sinusoidal voltage to the electromagnetic coil. The gain between the commanded MATLAB signal and the measured output voltage from the sound card is 2.44 in the frequency range of 20–250 Hz.

The amplitudes of the resulting force and torque are proportional to current i that flows through the middle coil of the Omnimagnet. To verify the expected linear relationship between input current and the resulting force and torque, we characterized the device by measuring the static force and torque on a permanent magnet in the same location used in our study. We used an ATI Nano17 six-axis force/torque sensor with a National Instruments PCIe 6320 data acquisition card

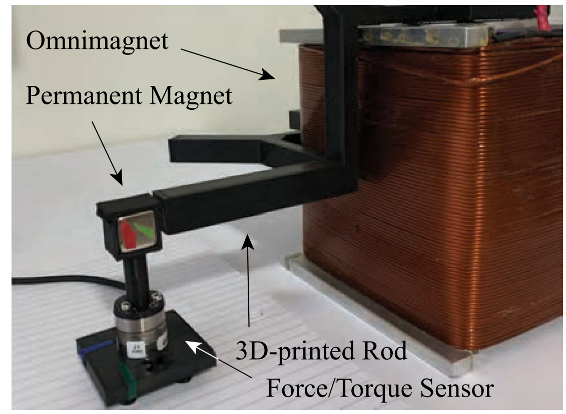

Fig. 14. Experimental setup for characterizing quasistatic force and torque. A permanent magnet is rigidly connected to a force/torque sensor using a 3D-printed fixture at the desired location. The distance between the center of the permanent magnet and the center of the Omnimagnet is 0.16 m.

with a 1 kHz sampling rate. We fabricated a custom fixture that rigidly fixed the permanent magnet of the device directly above the sensor (see Fig. 14), with the device in the configurations used during the human-subject studies (Fig. 4). In those studies we consider six configurations corresponding to six orthogonal modes, but magnetically there are just two distinct configurations used: pure force and pure torque. As shown in Fig. 4, a pure-force configuration happens when the dipole of the permanent magnet is parallel to the dipole of the Omnimagnet, and a pure-torque configuration happens when the direction of the permanent magnet is orthogonal to the dipole of the Omnimagnet; by changing the location and orientation of the stylus (including how the permanent magnet is attached to it) and the orientation of the Omnimagnet, we can direct force or torque in the desired direction (i.e., in each of the three orthogonal axes). To characterize force and torque as a function of current, we consider these two distinct configurations. We commanded DC current throughout the range of 0.5–4.5 A with a 0.5 A increment. We gathered data for five runs at 5 s of data per run. Before each run we gather 3 s of data, which is averaged and subtracted off to remove any bias from the measurements.

Figure 15 shows the measured force and torque in the configurations intended to generate pure force f_x or pure torque τ_x; linear least-squares regressions are also shown. In each linear fit, the offset term represents the best estimate of the bias in the force sensor used to gather the data, and the slope represents the best estimate of the actual force/torque generated by the haptic interface, which is known *a priori* to be linear with respect to current i [41]. In the pure-force configuration, the measured value was $f_x = 5.94i$ mN/A, whereas the model-based value was $f_x = 6.07i$ mN/A (i.e., the model overestimated by 3%). This discrepancy is due in part to the model assuming the magnet is touching the 3D-printed rod in Fig. 14, whereas during the actual experiments (and when used in the human-subjects studies) there was a small air gap between the magnet and the rod. In the pure-torque configuration, the measured value was $\tau_x = 0.302i$ mN $\cdot$ m/A, whereas the model-based value was $\tau_x = 0.310i$ mN $\cdot$ m/A (i.e., the model overestimated by 3%).

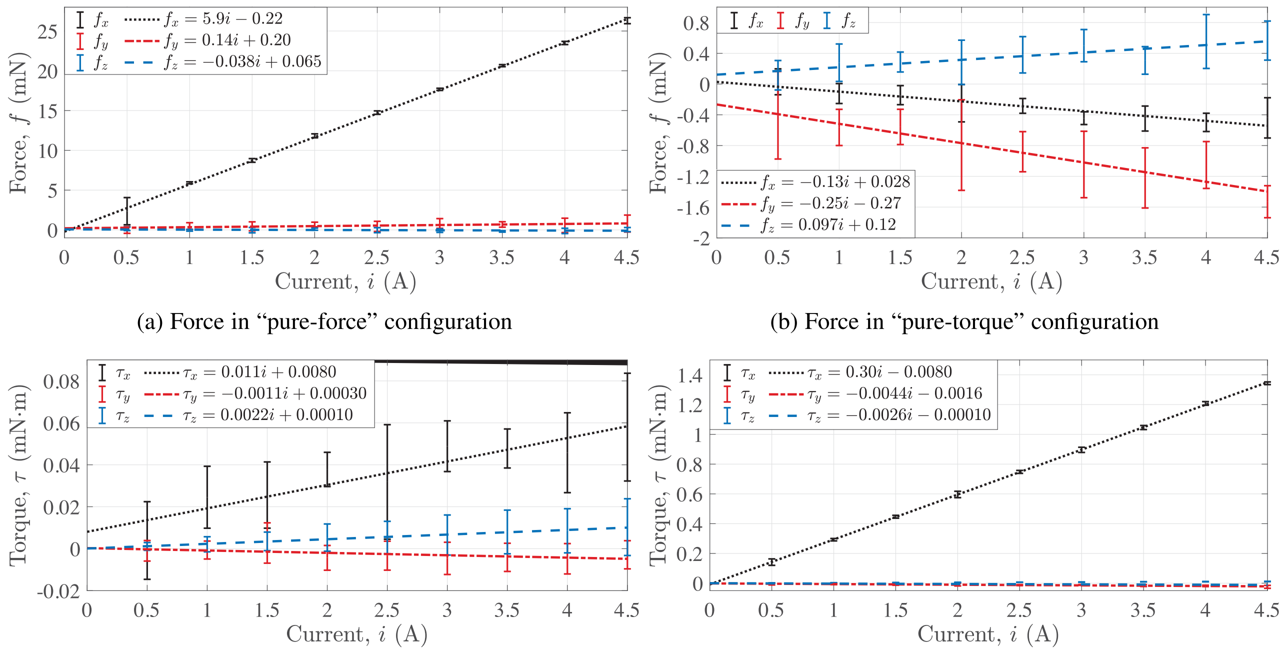

(a) Force in “pure-force” configuration

(b) Force in “pure-torque” configuration

(c) Torque in “pure-force” configuration

(d) Torque in “pure-torque” configuration

Fig. 15. The measured (means with 95% CI) and least-squares regression of static force and torque values as a function of constant current input in the configurations intended to generate pure force f_x or pure torque τ_x.

Let us consider the effect of the confounding force-torque components at the threshold detection values of $\tilde{f}_x$ and $\tilde{\tau}_x$, individually. Over the entire frequency range of interest, using the BET values from Fig. 7, we constructed the W matrix in (17), and then calculated $\tilde{P}$ from (16) using the respective values from Fig. 15 to form the V used in (16) at the i valued needed to achieve the desired $\tilde{f}_x$ or $\tilde{\tau}_x$, respectively. At each frequency, we computed the error in $\tilde{P}$ from the expected value of $\tilde{P} = 1$. We found that the maximum error was $|\tilde{P} - 1|/1 = 0.059$, which occurred at the frequency of 108 Hz, where subjects are most sensitive. This value is much lower than the most-conservative Weber fraction of 0.2 in intensity of vibrotactile stimuli reported in the literature [22], [43], [44]. This suggests that the confounding force-torque components are not of sufficient magnitude to impact our study.

Acknowledgment

The authors would like to thank Lan N. Pham for gathering the data in Figs. 14 and 15.

References

[1] A. M. Okamura, M. R. Cutkosky, and J. T. Dennerlein, “Reality-based models for vibration feedback in virtual environments,” *IEEE/ASME Trans. Mechatronics*, vol. 6, no. 3, pp. 245–252, Sep. 2001.

[2] K. J. Kuchenbecker, J. Fiene, and G. Niemeyer, “Improving contact realism through event-based haptic feedback,” *IEEE Trans. Vis. Comput. Graph.*, vol. 12, no. 2, pp. 219–230, Mar.–Apr. 2006.

[3] S. Choi and H. Z. Tan, “Toward realistic haptic rendering of surface textures,” *IEEE Comput. Graph. Appl.*, vol. 24, no. 2, pp. 40–47, Mar.–Apr. 2004.

[4] H. Culbertson, J. Unwin, and K. J. Kuchenbecker, “Modeling and rendering realistic textures from unconstrained tool-surface interactions,” *IEEE Trans. Haptics*, vol. 7, no. 3, pp. 381–393, Jul.–Sep. 2014.

[5] S. A. Pedram, R. L. Klatzky, and P. Berkelman, “Torque contribution to haptic rendering of virtual textures,” *IEEE Trans. Haptics*, vol. 10, no. 4, pp. 567–579, Oct.–Dec. 2017.

[6] H. Culbertson, S. B. Schorr, and A. M. Okamura, “Haptics: The present and future of artificial touch sensation,” *Annu. Rev. Control, Robot., Auton. Syst.*, vol. 1, pp. 385–409, 2018.

[7] S. Choi and H. Z. Tan, “Perceived instability of virtual haptic texture. i. experimental studies,” *Presence, Teleoperators Virtual Environ.*, vol. 13, no. 4, pp. 395–415, 2004.

[8] S. Choi and H. Z. Tan, “Perceived instability of virtual haptic texture: III. effect of update rate,” *Presence, Teleoperators Virtual Environ.*, vol. 16, no. 3, pp. 263–278, 2007.

[9] S. A. Cholewiak, K. Kim, H. Z. Tan, and B. D. Adelstein, “A frequency-domain analysis of haptic gratings,” *IEEE Trans. Haptics*, vol. 3, no. 1, pp. 3–14, Jan.–Mar. 2010.

[10] S. Shin and S. Choi, “Geometry-based haptic texture modeling and rendering using photometric stereo,” in *Proc. IEEE Haptics Symp.*, 2018, pp. 262–269.

[11] R. F. Friesen, R. L. Klatzky, M. A. Peshkin, and J. E. Colgate, “Single pitch perception of multi-frequency textures,” in *Proc. IEEE Haptics Symp.*, 2018, pp. 290–295.

[12] R. Zhang and J. J. Abbott, “Vibrotactile display of patterned surface textures with kinesthetic haptic devices using balanced impulses,” *IEEE Trans. Haptics*, to be publish, doi: 10.1109/TOH.2021.3072588.

[13] W. Nai, J. Liu, C. Sun, Q. Wang, G. Liu, and X. Sun, “Vibrotactile feedback rendering of patterned textures using a waveform segment table method,” *IEEE Trans. Haptics*, to be publish, doi: 10.1109/TOH.2021.3084304.

[14] S. Papetti and C. Saitis, Eds., *Musical Haptics*. Cham, Switzerland: Springer Open, 2018.

[15] B. Hannaford and A. M. Okamura, “Haptics,” in *Springer Handbook of Robotics*. Berlin/Heidelberg, Germany: Springer, 2016, pp. 1063–1084.

[16] M. C. Lin and M. Otaduy, *Haptic Rendering: Foundations, Algorithms, and Applications*. Boca Raton, FL, USA: CRC Press, 2008.

[17] J. R. Napier, “The prehensile movements of the human hand,” *J. Bone Joint*, vol. 38, no. 4, pp. 902–913, 1956.

[18] S. Choi and K. J. Kuchenbecker, “Vibrotactile display: Perception, technology, and applications,” *Proc. IEEE*, vol. 101, no. 9, pp. 2093–2104, 2013.

[19] S. J. Bolanowski Jr, G. A. Gescheider, R. T. Verrillo, and C. M. Checkosky, “Four channels mediate the mechanical aspects of touch,” *J. Acoust. Soc. Am.*, vol. 84, no. 5, pp. 1680–1694, 1988.

[20] A. Brisben, S. Hsiao, and K. Johnson, "Detection of vibration transmitted through an object grasped in the hand," *J. Neuriophysiol.*, vol. 81, no. 4, pp. 1548–1558, 1999.
[21] A. Israr, S. Choi, and H. Z. Tan, "Detection threshold and mechanical impedance of the hand in a pen-hold posture," in *Proc. IEEE/RSJ Int. Conf. Intell. Robots Syst.*, 2006, pp. 472–477.
[22] G. A. Gescheider, *Psychophysics: The Fundamentals*. New Jersey, NJ, USA: Psychol. Press, Mahwah, 2013.
[23] N. Landin, J. M. Romano, W. McMahan, and K. J. Kuchenbecker, "Dimensional reduction of high-frequency accelerations for haptic rendering," in *Proc. Int. Conf. Hum. Haptic Sens. Touch Enabled Comput*. Appl., 2010, pp. 79–86.
[24] L. A. Jones and S. J. Lederman, *Human Hand Function*. London, U.K.: Oxford Univ. Press, 2006.
[25] M. Strese, J.-Y. Lee, C. Schuwerk, Q. Han, H.-G. Kim, and E. Steinbach, "A haptic texture database for tool-mediated texture recognition and classification," in *Proc. IEEE Haptic Symp.*, 2014, pp. 118–123.
[26] H. Culbertson, J. J. L. Delgado, and K. J. Kuchenbecker, "One hundred data-driven haptic texture models and open-source methods for rendering on 3D objects," in *Proc. IEEE Haptics Symp.*, 2014, pp. 319–325.
[27] J. Z. Wu, D. E. Welcome, K. Krajnak, and R. G. Dong, "Finite element analysis of the penetrations of shear and normal vibrations into the soft tissues in a fingertip," *Med. Eng. Phys.*, vol. 29, no. 6, pp. 718–727, 2007.
[28] K. J. Kuchenbecker *et al.*, "Characterizing the human wrist for improved haptic interaction," in *Proc. ASME Int. Mech. Eng. Congr. Expo.*, 2003, pp. 591–598.
[29] W. McMahan and K. J. Kuchenbecker, "Haptic display of realistic tool contact via dynamically compensated control of a dedicated actuator," in *Proc. IEEE/RSJ Int. Conf. Intell. Robots Syst.*, 2009, pp. 3170–3177.
[30] T. Tsuji, "Human arm impedance in multi-joint movements," in *Adv. Psychol*. Elsevier, 1997, vol. 119, pp. 357–381.
[31] R. G. Dong, J. H. Dong, J. Z. Wu, and S. Rakheja, "Modeling of biodynamic responses distributed at the fingers and the palm of the human hand-arm system," *J. Biomech.*, vol. 40, no. 10, pp. 2335–2340, 2007.
[32] H. S. Woo and D. Y. Lee, "Exploitation of the impedance and characteristics of the human arm in the design of haptic interfaces," *IEEE Trans. Ind. Electron.*, vol. 58, no. 8, pp. 3221–3233, Aug. 2011.
[33] M. J. Fu and M. C. Çavuşoğlu, "Human-arm-and-hand-dynamic model with variability analyses for a stylus-based haptic interface," *IEEE Trans. Systems, Man, Cybern., Part B. Cybern.*, vol. 42, no. 6, pp. 1633–1644, Dec. 2012.
[34] I. Hwang, J. Seo, M. Kim, and S. Choi, "Vibrotactile perceived intensity for mobile devices as a function of direction, amplitude, and frequency," *IEEE Trans. Haptics*, vol. 6, no. 3, pp. 352–362, Jul.–Sep. 2013.
[35] G. Park and K. J. Kuchenbecker, "Objective and subjective assessment of algorithms for reducing three-axis vibrations to one-axis vibrations," in *Proc. IEEE World Haptics Conf.*, 2019, pp. 467–472.
[36] R. Zhang, A. J. Boyles, and J. J. Abbott, "Six principal modes of vibrotactile display via stylus," in *Proc. IEEE Haptics Symp.*, 2018, pp. 313–318.
[37] R. Zhang, T. J. Schwehr, and J. J. Abbott, "Addendum to 'dimensional reduction for 6D vibrotactile display'," *IEEE Trans. Haptics*, vol. 14, no. 2, pp. 445–448, Apr.–Jun. 2021.
[38] R. Zhang, T. J. Schwehr, and J. J. Abbott, "Dimensional reduction for 6D vibrotactile display," *IEEE Trans. Haptics*, vol. 13, no. 1, pp. 102–108, Jan.–Mar. 2020.
[39] J. Bell, S. Bolanowski, and M. H. Holmes, "The structure and function of pacinian corpuscles: A review," *Prog. Neurobiol.*, vol. 42, no. 1, pp. 79–128, 1994.
[40] C. Salisbury, R. B. Gillespie, H. Z. Tan, F. Barbagli, and J. K. Salisbury, "What you can't feel won't hurt you: Evaluating haptic hardware using a haptic contrast sensitivity function," *IEEE Trans. Haptics*, vol. 4, no. 2, pp. 134–146, Apr.–Jun. 2011.
[41] J. J. Abbott, E. Diller, and A. J. Petruska, "Magnetic methods in robotics," *Annu. Rev. Control Robot. Auton. Syst.*, vol. 3, pp. 57–90, 2020.
[42] S. S. Stevens, "On the psychophysical law," *Psychol. Rev.*, vol. 64, no. 3, pp. 153–181, 1957.
[43] J. C. Craig, "Difference threshold for intensity of tactile stimuli," *Percep. Psychophys.*, vol. 11, no. 2, pp. 150–152, 1972.
[44] J. C. Craig, "Vibrotactile difference thresholds for intensity and the effect of a masking stimulus," *Percep. Psychophys.*, vol. 15, no. 1, pp. 123–127, 1974.
[45] D. Fucci, L. H. Small, and L. Petrosino, "Intensity difference limens for lingual vibrotactile stimuli," *Bull. Psychon. Soc.*, vol. 20, no. 1, pp. 54–56, 1982.
[46] R. T. Verrillo and G. A. Gescheider, "Perception via the sense of touch," in *Tactile Aids Hear. Impaired*, Whurr, London, U.K., 1992, pp. 1–36.
[47] A. Israr, H. Z. Tan, and C. M. Reed, "Frequency and amplitude discrimination along the kinesthetic-cutaneous continuum in the presence of masking stimuli," *J. Acoust. Soc. Am.*, vol. 120, no. 5, pp. 2789–2800, 2006.
[48] H. R. Dinse, P. Ragert, B. Pleger, P. Schwenkreis, and M. Tegenthoff, "Pharmacological modulation of perceptual learning and associated cortical reorganization," *Science*, vol. 301, no. 5629, pp. 91–94, 2003.
[49] D. M. Green, "Stimulus selection in adaptive psychophysical procedures," *J. Acoust. Soc. Am.*, vol. 87, no. 6, pp. 2662–2674, 1990.
[50] H. Levitt, "Transformed up-down methods in psychoacoustics," *J. Acoust. Soc. Am.*, vol. 49, no. 2B, pp. 467–477, 1971.
[51] M. C. Meilgaard, B. T. Carr, and G. V. Civille, *Sensory Evaluation Techniques*. Boca Raton, FL, USA: CRC Press, 2006.
[52] A. J. Petruska and J. J. Abbott, "Omnimagnet: An omnidirectional electromagnet for controlled dipole-field generation," *IEEE Trans. Magn.*, vol. 50, no. 7, pp. 1–10, Jul. 2014.

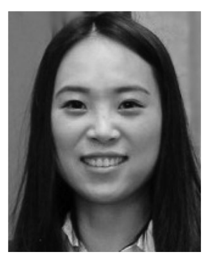

Ruisi Zhang (Student Member, IEEE) received the B.S. and M.S. degrees in mechanical engineering from Iowa State University, Ames, IA, USA, in 2012 and 2013, respectively, and the Ph.D. degree in mechanical engineering from the University of Utah, Salt Lake City, UT, USA, in 2021.

From 2014 to 2015, she was a Research Intern with the Institute of Computing Technology, Chinese Academy of Sciences, Beijing, China. In 2021, she became a Postdoctoral Researcher with Brigham and Women's Hospital, Harvard Medical School, Boston, MA, USA.

Jake J. Abbott (Senior Member, IEEE) received the B.S. degree in mechanical engineering from Utah State University, Logan, UT, USA, in 1999, the M.S. degree in mechanical engineering from the University of Utah, Salt Lake City, UT, USA, in 2001, and the Ph.D. degree in mechanical engineering from Johns Hopkins University, Baltimore, MD, USA, in 2006.

In 2006, he became a Postdoctoral Researcher with ETH Zurich, Switzerland. In 2008, he joined the Department of Mechanical Engineering, University of Utah, where he is currently a Professor.